

X-ray Synchrotron Spectral Hardenings from Compton and Synchrotron Losses in Extended Chandra Jets

Charles D. Dermer¹ and Armen M. Atoyan²

ABSTRACT

Chandra observations of knots and hot spots in spatially resolved X-ray jets of radio galaxies show that the X-ray fluxes often lie above an extrapolation from the radio-to-optical continuum fluxes. We show that combined synchrotron and Compton losses on a single power-law electron injection function can produce a hardening in the electron spectrum at electron Lorentz factors $\gamma \approx 2 \times 10^8 / [\Gamma(1+z)]$ due to KN energy losses on the cosmic microwave background radiation. Here Γ is the bulk Lorentz factor of the outflow, and z is the source redshift. This produces a flattening in the spectrum at frequencies $\gtrsim 8 \times 10^{16} \delta B_{\mu G} / [\Gamma^2(1+z)^3]$ Hz, where $B_{\mu G}$ is the magnetic field in the comoving plasma frame in units of micro-Gauss and δ is the Doppler factor. A single population of synchrotron-emitting electrons may therefore produce the radio-to-X-ray continuum in some radio galaxy knots, such as those in 3C 273.

Subject headings: galaxies: active — galaxies: jets — gamma-rays: theory — radiation mechanisms: nonthermal — X-rays: galaxies

1. Introduction

The excellent spatial resolution of the *Chandra X-ray Observatory* is providing X-ray images of extended radio galaxy jets in the 0.2-8 keV band at resolutions better than 0.4'' FWHM, and spectral detail of discrete components at flux levels between $\approx 10^{-13}$ and 10^{-14} ergs cm $^{-2}$ s $^{-1}$. Combined with high resolution radio and optical maps, spectral energy distributions (SEDs) of spatially-resolved hot spots and knots in the jets of radio galaxies can be studied from the radio through the X-ray regime.

¹E. O. Hulbert Center for Space Research, Code 7653, Naval Research Laboratory, Washington, DC 20375-5352

²CRM, Universite de Montreal, Montreal H3C 3J7, Canada

The broadband SEDs in many of the hot spots and knots show a general behavior whereby the X-ray spectra are harder than the optical spectra, and the X-ray fluxes are above an extrapolation from the optical fluxes. This behavior is observed in the SEDs of at least three of the four regions along the X-ray jet of 3C 273 (Sambruna et al. 2001; Marshall et al. 2001), the western hot spot of Pictor A (Wilson, Young, and Shopbell 2001), knot WK7.8 of PKS 0637-752 (Schwartz et al. 2000; Chartas et al. 2000), hot spot A of Cygnus A (Wilson, Young, and Shopbell 2000), and in some of the knots in the jet of M87 (Wilson & Yang 2001). In other cases, such as the X-ray jet in 3C 66B (Hardcastle, Birkinshaw, & Worrall 2001), knots A1 and A3 in 3C 273 (Marshall et al. (2001); see, however, Sambruna et al. (2001) for a different spectral analysis), and some other knots in M87’s jet (Wilson & Yang 2001), the X-ray–optical–radio spectrum is consistent with a single or smoothly broken power-law spectrum, indicating that the broadband emission is entirely due to nonthermal synchrotron radiation.

Three main leptonic processes have been considered to account for the X-ray emission in the extended jets (e.g., Harris and Krawczynski 2002): nonthermal synchrotron radiation, synchrotron self-Compton (SSC) radiation, and X-ray emission from Compton-scattered external radiation fields. Nonthermal synchrotron emission is favored for smooth spectra and for the western hot spot of Pictor A (Wilson, Young, and Shopbell 2001), where an SSC origin implies a very weak magnetic field, and a combined SSC/synchrotron origin requires that the two emission components be carefully matched in the X-ray regime. The SSC process can, however, explain the X-ray emission mechanism from the bright radio hot spots of Cygnus A (Wilson, Young, and Shopbell 2000), the radio hot spots of 3C 295 (Harris et al. 2000), and the eastern hot spot of 3C 123 (Hardcastle, Birkinshaw, & Worrall 2001a).

Tavecchio et al. (2000) and Celotti, Ghisellini, & Chiaberge (2001) argue that the X-ray emission from knot WK7.8 is due to Compton-scattered cosmic microwave background radiation (CMBR) rather than to SSC emission, because an SSC model requires a system well out of equilibrium and a jet that is significantly debeamed. This model invokes an emitting region in bulk relativistic motion on size scales of several hundred kpc, in accord with observations of one-sidedness in the jets on these size scales. Such a model has been applied to X-ray emitting knots in the jet of 3C 273 by Sambruna et al. (2001). A synchrotron model for the X-ray emission is discounted because it would apparently require two populations of relativistic electrons to explain the radio, optical, and X-ray fluxes. Another possibility is that the X-rays are synchrotron radiation of high-energy protons (Aharonian 2001).

Here we show that synchrotron emission from a single population of electrons injected with a nonthermal power law spectrum can produce X-ray spectral hardenings. When CMBR cooling in the Thomson regime exceeds synchrotron cooling, a hardening in the electron

spectrum is formed at electron energies where KN effects become important. This produces a hardening in the synchrotron spectrum between optical and X-ray frequencies. In the next section, an analytic model for the synchrotron origin of X-ray emission from extended jets is presented, motivated by Chandra observations of 3C 273. Results of a numerical simulation with cascade reprocessing are given in Section 3. Section 4 gives a discussion and summary.

2. Analytic Model

In 3C 273, the X-ray energy spectral index in the inner knot region A has $\alpha_x \sim 1.1$, a value characteristic of a cooling shock-accelerated electron spectrum, and there is an indication of spectral softening along the jet (Sambruna et al. 2001). The peaks of the X-ray emission along the jet of 3C 273 closely track the peaks in the optical waveband, and the overall X-ray emission profile displays a decreasing mean intensity along the jet, whereas the optical intensity is roughly uniform along the jet. The radio profile also displays brightenings in spatial coincidence with the X-ray and optical peaks, but the radio intensity increases dramatically along the jet. The optical emission profiles are narrower than those of the radio emission.

These behaviors suggest that the electron population producing the radio emission accumulates due to weak cooling, whereas the electrons producing the optical and X-ray emission strongly cool. Electrons that produce synchrotron radio emission at observer’s frame frequencies ν have Lorentz factors $\gamma \approx 5 \times 10^4 [(\nu/5 \text{ GHz})(1+z)/\delta B_{\mu\text{G}}]^{1/2}$, whereas the electrons that Compton scatter the CMBR to X-ray energies E_x have $\gamma \approx 1 \times 10^3 [(E_x/1 \text{ keV})/\delta\Gamma]^{1/2}$. Consequently the X-ray emitting electrons will cool more slowly than the radio-emitting electrons unless B exceeds milli-Gauss intensities. The fast-cooling requirement for the X-ray emitting electrons is readily satisfied assuming a synchrotron origin for the X-rays. In this paper, we neglect complications that involve variations of the magnetic field B and the Doppler factor $\delta = [\Gamma(1 - \beta_{\Gamma} \cos \theta)]^{-1}$ along the length of the jet. (Here $\beta_{\Gamma} = (1 - \Gamma^{-2})^{-1/2}$ and θ is the angle between the directions of the jet and the observer.)

The synchrotron energy-loss rate of relativistic nonthermal electrons with a random pitch-angle distribution in a region with comoving mean intensity B is $-\dot{\gamma}_{syn} \cong 1.3 \times 10^{-21} B_{\mu\text{G}}^2 \gamma^2 \text{ s}^{-1} \equiv k_{syn} \gamma^2$ (Blumenthal & Gould 1970). Under the same conditions, the energy loss rate due to Compton-scattered CMB radiation in the Thomson limit is $-\dot{\gamma}_T = (4c\sigma_T/3m_e c^2)\gamma^2(1+z)^4 \hat{u}_{CMB}\Gamma^2(1 + \beta_{\Gamma}^2/3) \cong 1.7 \times 10^{-20} \gamma^2(1+z)^4 \Gamma^2 \text{ s}^{-1} \equiv k_T \gamma^2$, where $\hat{u}_{CMB} \cong 4 \times 10^{-13} \text{ ergs cm}^{-3}$ is the local ($z = 0$) intensity of the CMBR. This expression holds when $\gamma \ll \gamma_{KN}$, where γ_{KN} is the Lorentz factor above which KN effects become important, given through $4\gamma_{KN}\hat{\epsilon}' = 1$. For the CMB radiation, the dimensionless mean photon

energy $\hat{\epsilon}' \cong \hat{\epsilon}_{CMB}\Gamma(1+z) \cong 2.7(k_B \times 2.72\text{K})\Gamma(1+z)/m_e c^2$ and $\hat{\epsilon}_{CMB} = 1.24 \times 10^{-9}$, so that electrons with $\gamma \ll \gamma_{KN} = 2 \times 10^8/\Gamma(1+z)$ scatter CMB radiation in the Thomson regime.

In the extreme KN limit, the electron energy loss rate $-\dot{\gamma}_{KN} \cong 4.6 \times 10^{-3}(1+z)^2 \ln[2.54\gamma_{10}\Gamma(1+z)] \text{ s}^{-1}$ (Blumenthal & Gould 1970), where $\gamma_{10} = \gamma/10^{10}$, and $\Theta = k_B(2.72)(1+z)/m_e c^2 = 4.6 \times 10^{-10}(1+z)$ is the dimensionless temperature. We approximate the combined energy-loss rate for analytic simplicity by the expression

$$-\dot{\gamma} = [k_{syn} + \frac{k_T}{1 + (a\gamma/\gamma_{KN})^b}] \gamma^2 \equiv K_{synC}(\gamma) \gamma^2, \quad (1)$$

where $a = 0.5$ and $b = 1.7$ are chosen to fit roughly the $-\dot{\gamma} \propto \ln \gamma$ behavior in the extreme KN regime and to provide spectral results within a factor $\sim 2\text{-}3$ of the numerical results. Equation (1) shows that when $k_T \gg k_{syn}$, $\dot{\gamma}$ is dominated by Thomson losses at $\gamma \ll \gamma_{KN}$, $\dot{\gamma}$ flattens at $\gamma_{KN} \lesssim \gamma \lesssim \bar{\gamma} = \gamma_{KN} \sqrt{k_T/k_{syn}} \equiv \gamma_{KN} \sqrt{N_{Ts}}$, and $\dot{\gamma}$ is dominated by synchrotron losses at $\gamma \gg \bar{\gamma}$. Adiabatic losses are neglected here but can be shown to be negligible for X-ray emitting electrons.

For numerical calculations in the next section, we solve the time-dependent continuity equation for the energy spectrum of electrons $N_e(\gamma, t)$ injected in the source with differential injection rate $Q(\gamma, t)$. For the analytic model treated here, we approximate the injection rate as a stationary function starting from $t_0 = 0$, with a single power-law behavior $Q(\gamma) = Q_0 \gamma^{-p} \exp(-\gamma/\gamma_{max})$ for $\gamma \geq \gamma_{min}$, implying a comoving frame electron power $L_e = m_e c^2 \int_{\gamma_{min}}^{\gamma_{max}} d\gamma \gamma Q(\gamma)$. In the stationary injection case with $p > 1$, the energy distribution of electrons at time t can be approximated by $N_e(\gamma, t) \cong Q(\gamma) t_{ac}$, where the characteristic electron accumulation time $t_{ac} = \min(t, t_{cool} = -\gamma/\dot{\gamma})$. In this approximation

$$\gamma^3 N_e(\gamma) \cong Q_0 \begin{cases} \frac{\gamma^{3-p}}{[K_{synC}(\gamma_{cool})\gamma_{cool}]} , & \text{for } \gamma_{min} \lesssim \gamma \leq \gamma_{cool} \\ \frac{\gamma^{2-p}}{K_{synC}(\gamma)} , & \text{for } \gamma_{cool} \leq \gamma \lesssim \gamma_{max} \end{cases} \quad (2)$$

where $\gamma_{cool} \equiv \gamma_{cool}(t)$ is found from the equation $t_{cool}(\gamma_{cool}) = t$. Equation (2) applies when $\gamma_{min} < \gamma_{cool}$ and is easily generalized in the opposite case. We consider the case where $\gamma_{cool} \ll \gamma_{KN} \ll \gamma_{max}$, and $\gamma_{max} = \sqrt{3e_{max}e/\sigma_T B} \cong 4.6 \times 10^{10} \sqrt{e_{max}/B_{\mu\text{G}}}$ (e.g., de Jager et al. 1996), where the parameter $e_{max} \lesssim 1$.

In the δ -function approximation for the synchrotron and Thomson radiation processes, the νF_ν synchrotron radiation spectrum from a uniform blob, assumed spherical in the comoving frame, is

$$f_\epsilon^{syn} \cong \delta^4 \left(\frac{c\sigma_T u_B}{6\pi d_L^2} \right) \gamma_{syn}^3 N_e(\gamma_{syn}) , \quad (3)$$

where $\gamma_{syn} = \sqrt{(1+z)\epsilon/(\delta\epsilon_B)}$, d_L is the luminosity distance, $\epsilon = h\nu/m_ec^2$, and $\epsilon_B = B/4.414 \times 10^{13}$ G. The νF_ν Thomson radiation spectrum for an external isotropic monochromatic radiation field is

$$f_\epsilon^T \simeq \delta^6 \left(\frac{c\sigma_T u_*}{6\pi d_L^2} \right) \gamma_C^3 N_e(\gamma_C) \quad (4)$$

(Dermer et al. 1997; Dermer & Schlickeiser 2001). Here $\gamma_C = \delta^{-1} \sqrt{(1+z)\epsilon/(2\epsilon_*)}$, $\epsilon_* = \hat{\epsilon}_{CMB}(1+z)$ and $u_* = \hat{u}_{CMB}(1+z)^4$ are the mean photon energy and radiation energy density, respectively, of the ambient CMBR field in the stationary frame. An accurate representation of the Compton-scattered spectrum in the KN regime is given by Georganopoulos, Kirk, & Mastichiadis (2001).

The KN effects on the synchrotron spectrum are observed at $\nu_{KNs1}(\text{Hz}) \cong 2\delta B_{\mu\text{G}} \gamma_{KN}^2 / (1+z) \approx 8 \times 10^{16} \delta B_{\mu\text{G}} / [\Gamma^2 (1+z)^3]$. The reduction of Compton losses compared to the $-\dot{\gamma} \propto \gamma^2$ behavior hardens the electron spectrum until synchrotron losses dominate at $\gamma > \bar{\gamma}$, resulting again in a steepening of the synchrotron spectrum in the hard X-ray domain. The KN effects on the Compton-scattered CMBR spectrum are observed at dimensionless photon energy $\epsilon_{KNC} = h\nu_{KNC}/m_ec^2 \cong 10^8(\delta/\Gamma)(1+z)^{-2}$, implying a hardening in the photon spectrum at photon energy $E > E_{KNC} \cong 50(\delta/\Gamma)(1+z)^{-2}$ TeV. We set the normalization $Q_0 = (p-2)10^{44}L_{44} \text{ ergs s}^{-1} / [(m_ec^2)(\gamma_{min}^{2-p} - \gamma_{max}^{2-p})]$ and let $p = 2.3$, corresponding to the likely spectral index of particles accelerated by relativistic shocks (Achterberg et al. 2001).

Figs. 1a and 1b show two suites of models inspired by the Chandra data. In Fig. 1a, we assume that $\Gamma = 10$ in a nearby radio galaxy with $z = 0.15$. We also assume that the jet axis is inclined at an angle $\theta = 4/\Gamma = 23^\circ$. The comoving magnetic field ranges in values from 5 to 50 μG , and effects of different values of γ_{cool} are illustrated. A field of 44 μG gives equipartition between the magnetic-field and comoving CMBR energy densities. The spectral hardening between the optical and X-ray regimes is apparent. Note that the use of the δ -function approximation in the analytic approach enhances spectral features.

The $\Gamma = 10$ jet with $B_{\mu\text{G}} = 30$ and $\gamma_{cool} = 10^5$ is placed at $z = 1$ in Fig. 1b, but now with the outer jet oriented at various angles to the observer. The increasingly dominant Compton component at small angles results from the different beaming factors for synchrotron and Compton processes (Dermer 1995). For sufficiently small values of θ and γ_{min} , Thomson-scattered X-ray CMBR could make a significant or dominant contribution to knot and hot spot emission, as in knot WK7.8 of the $z = 0.651$ superluminal source PKS 0637-752, with apparent transverse speeds reaching $\approx 18c$ (Schwartz et al. 2000; Tavecchio et al. 2000). When observing too close within the beaming cone, the direct inner jet radiation may however dominate, which could result in a pattern of γ -ray flares superimposed on a significantly weaker but persistent (on time scales of thousands of years) flux.

3. Numerical Model

Numerical calculations are done using the well-known solution for the energy distribution $N_e(\gamma, t)$ of electrons suffering energy losses $P(\gamma) \equiv (-\dot{\gamma})$, which are contributed mostly by Compton and synchrotron losses. Calculations are done in the comoving frame of a source moving relativistically with Lorentz-factor Γ , and then the emerging radiation spectra are transformed to the observer frame. We neglect possible escape losses of accelerated particles. This is valid for the large characteristic size of the X-ray knots of order $R_{knot} \sim 1\text{-}10$ kpc or so, because for $\gamma > 10^4$ the electron cooling time $t_{cool} \lesssim 10^5$ yr in the comoving frame, which is smaller than any reasonable escape time from such a large source. Particle escape may be important in much smaller-scale inner jets of blazars (Atoyan & Dermer 2001, 2002) or jets of microquasars (Atoyan & Aharonian 1999).

Gamma rays with energies $\gtrsim 10^{15}\Gamma^{-1}(1+z)^{-1}$ eV could be absorbed in $\gamma\gamma$ collisions with the CMB photons inside the source. This process provides an injection function $Q_{1,\gamma\gamma}(\gamma, t)$ for the first generation electrons (e^+, e^-) of the pair-photon cascade, which we also take into account in our calculations. Note however that the cascade radiation turns out to be insignificant compared with the radiation from the main injection $Q(\gamma, t)$ unless a large fraction of the overall power is injected at electron energies $\gtrsim 100$ TeV (Atoyan & Dermer 2002).

We consider an electron injection spectrum

$$Q(\gamma, t) \simeq \gamma^{-p} e^{-\gamma/\gamma_{max}} (1 + t/t_{inj})^{-q} \quad (5)$$

at energies $\gamma_{min} < \gamma$ extending with index $p = 2.3$ to PeV energies, and we set $\gamma_{max} = 2 \times 10^9$. The injection function is approximated by $Q \propto (\gamma/\gamma_{cool})^2$ at $\gamma \lesssim \gamma_{min} = \gamma_0\Gamma$ with $\gamma_0 = 300$. Note that for electron acceleration by relativistic shocks, the values of γ_0 could reach a large fraction of $(m_p/m_e)\Gamma \sim 2000\Gamma$. The time profile of the injection in equation (5) treats both stationary (at $t \geq 0$) injection if $t_{inj} \gg t$, as well as gradually declining injection at $t_{inj} \lesssim t$, when $q > 0$.

In Fig. 2a we show the synchrotron and Compton fluxes expected from a relativistic knot with $\Gamma = 10$ in a distant blazar at $z = 1$ for three different times in the knot frame: $t' = 10^4$ yr, 5×10^4 yr, and 3×10^5 yr. If the injection starts relatively close to the core, then these timescales would effectively correspond to knots at distances $l = ct'\Gamma \simeq 33$ kpc, 166 kpc, and ~ 1 Mpc from the core. Injection is assumed to be stationary with $L_{44} = 1$, and the magnetic field and the jet angle to the observer are $B = 30 \mu\text{G}$ and $\theta = 11.4^\circ$ respectively. Fig. 2b shows the fluxes expected at the same epochs t' from a closer blazar at $z = 0.15$, calculated for a smaller magnetic field $B = 6 \mu\text{G}$ and $\Gamma = 5$, and with $\theta = 23^\circ$. The electron injection here is assumed to decline with $q = 1/2$ and with a characteristic

timescale $t_{inj} = 5 \times 10^3$ yr, for initial power $L_{44} = 5$. Fig. 2b demonstrates that the X-ray and optical fluxes may significantly drop while the radio flux continues to rise with increasing distance, as observed in 3C 273 (Sambruna et al. 2001). At the same time, the X-ray fluxes may be systematically harder than the optical spectra, again in qualitative agreement with observations of 3C 273.

4. Discussion and Summary

We have shown that the combined effects of Compton and synchrotron losses on a power-law electron injection spectrum can produce a hardening between the optical and X-ray regimes. This model is in accord with observations of X-ray spectral hardenings in the knots of 3C 273 (Sambruna et al. 2001; Marshall et al. 2001) and other sources, suggesting that the X-ray emission is due to a cooling spectrum of electrons accelerated by a strong shock. In a synchrotron model for the X-rays, the X-ray profiles are narrower than radio profiles, because the X-rays are emitted by higher energy electrons and therefore cool more rapidly than the radio-synchrotron emitting electrons.

The Thomson energy-loss rate must exceed the synchrotron energy loss-rate to produce X-ray spectral hardenings, so a large fraction of the energy in nonthermal electrons is radiated as γ -rays with energies $\gtrsim 50(\delta/\Gamma)(1+z)^{-2}$ TeV. The Compton-scattered CMB radiation from the knots and hot spots make nearly aligned extended jet sources potentially detectable with *GLAST* and the next generation of ground-based air Cherenkov γ -ray telescopes such as VERITAS, HESS, and MAGIC. The relative intensities of the X-ray and γ -ray fluxes can be used to infer δ , but the limited spatial resolution of gamma-ray telescopes will pose difficulties in separating core jet components (excepting those which are highly variable) from steady extended emission components. SIRTF will be important to offer greater spectral detail about the synchrotron component, and to correlate spectral-cooling breaks in the synchrotron component with the break in the Thomson component observed with *GLAST*.

The CMB radiation scattered in the Klein-Nishina regime will provide a source of ultra-high energy gamma-rays that can pair produce in the diffuse CMB and infrared radiation fields to form pair halos (Aharonian, Coppi, & Völk 1994), as well as providing a source of synchrotron-emitting electrons. The mean-free-path for $\gamma\gamma$ attenuation in the CMB reaches a minimum value of $\cong 8$ kpc/(1+z)³ at observed photon energies $E_\gamma \cong 1$ PeV, and increases to Mpc scales at lower and higher energies. In the model of Atoyan & Dermer (2001, 2002), the injection of energy into the extended jets of FRII radio galaxies is a consequence of neutral beams composed of ultra-high energy neutrons and γ -rays ($\sim 10^{13.5}$ - 10^{18} eV) formed through photomeson production in the inner jet, explaining the colinearity of the inner and

extended jets up to Mpc scales. The highly collimated neutral-beam energy is deposited in the intergalactic medium to drive relativistic outflows and form shocks that accelerate high-energy particles which radiate X-ray emission observed with Chandra.

We thank Hui Li for discussions about the synchrotron radiation from high-energy pair cascades, Andrew Wilson for discussions about the *Chandra* data, and the referee for a useful report. AA appreciates the hospitality and support of the NRL Gamma and Cosmic Ray (now High Energy Space Environment) Branch during his visit when this work has been done. The work of CD is supported by the Office of Naval Research and NASA grant No. DPR S-13756G.

REFERENCES

Achterberg, A., Gallant, Y. A., Kirk, J. G., & Guthmann, A. W. 2001, MNRAS, 328, 393

Aharonian, F. A., Coppi, P. S., & Völk, H. J. 1994, ApJ, 423, L5

Aharonian, F. A. 2001, MNRAS, submmitted (astro-ph/0106037)

Atoyan, A. M., & Aharonian, F. A. 1999, MNRAS, 302, 253

Atoyan, A., & Dermer, C. D. 2001, Phys. Rev. Lett., 87, 221102

Atoyan, A. M., & Dermer, C. D. 2002, in preparation

Blumenthal, G. R. & Gould, R. J. 1970, Reviews of Modern Physics, 42, 237

Celotti, A., Ghisellini, G., & Chiaberge, M. 2001, MNRAS, 321, L1

Chartas, G., et al. 2000, ApJ, 542, 655

Dermer, C. D. 1995, ApJ, 446, L63

Dermer, C. D., Sturner, S. J., and Schlickeiser, R. 1993, ApJS, 109, 103

Dermer, C. D. & Schlickeiser, R. 2001, ApJ, submitted (astro-ph/0202280)

Georganopoulos, M., Kirk, J. G., & Mastichiadis, A. 2001, ApJ, 561, 111

Hardcastle, M. J., Birkinshaw, M., & Worrall, D. M. 2001, MNRAS, 326, 1499

Hardcastle, M. J., Birkinshaw, M., & Worrall, D. M. 2001a, MNRAS, 323, L17

Harris, D. E. et al. 2000, *ApJ*, 530, L81

Harris, D. E., & Krawczynski, H. 2002, *ApJ*, 565, 244

de Jager, O. C., Harding, A. K., Michelson, P. F., Nel, H. I., Nolan, P. L., Sreekumar, P., & Thompson, D. J. 1996, *ApJ*, 457, 253

Marshall, H. L., et al. 2001, *ApJ*, 549, L167

Sambruna, R., Urry, C. M., Tavecchio, F., Maraschi, L., Scarpa, R., Chartas, G., and Muxlow, T. 2000, *ApJ*, 549, L61

Schwartz, D. A., et al. 2000, *ApJ*, 540, L69

Tavecchio, F., Maraschi, L., Sambruna, R. M., and Urry, C. M., 2000, *ApJ*, 544, L23

Wilson, A. S., Young, A. J., and Shopbell, P. L. 2001, *ApJ*, 547, 740

Wilson, A. S., Young, A. J., and Shopbell, P. L. 2000, *ApJ*, 544, L27

Wilson, A. S., and Yang, Y. 2001, *ApJ*, in press (astro-ph/0112097)

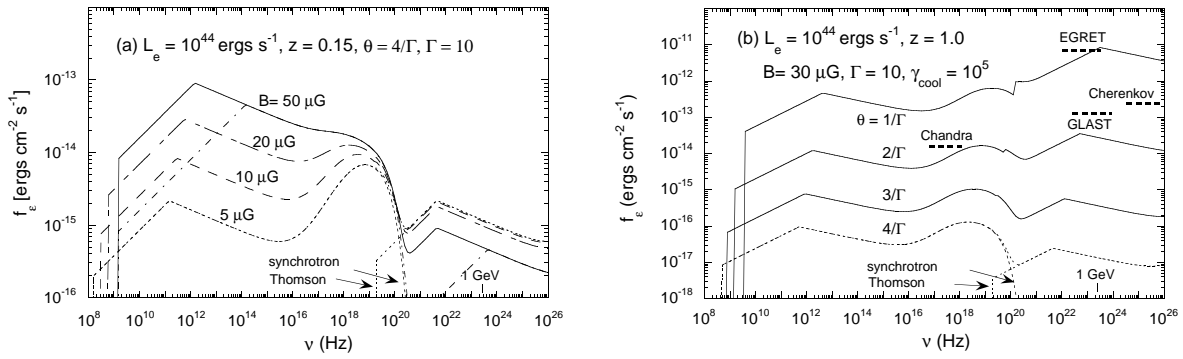


Fig. 1.— Analytic model SEDs radiated by a relativistic magnetized knot energized by stationary relativistic power-law electron injection. The electrons are subject to synchrotron losses and Compton losses with CMB photons. (a) The source is at redshift $z = 0.15$, and the jet is oriented at $\theta = 4/\Gamma$, with bulk Lorentz factor $\Gamma = 10$ and different comoving magnetic fields as labeled. Separate synchrotron and Thomson components are shown in the $B_{\mu\text{G}} = 5$ case. The value of $\gamma_{\text{cool}} = 10^5$ except for the dot-dashed curve, where $\gamma_{\text{cool}} = 10^6$. The injection power in nonthermal electrons is $L_e = 10^{44} \text{ ergs s}^{-1}$ ($L_{44} = 1$), $\gamma_{\min} = 3000$, and $e_{\max} = 0.01$. (b) Analytic model SEDs of a source at $z = 1$ ($d_L = 2.2 \times 10^{28} \text{ cm}$) with $\Gamma = 10$, $B_{\mu\text{G}} = 30$, $e_{\max} = 0.01$, and $\gamma_{\text{cool}} = 10^5$. Effects of changes in the angle between the jet and observer directions are shown. Rough sensitivities for EGRET and GLAST in a 1-year survey, the sensitivity for Chandra from published analyses, and the anticipated sensitivity of next-generation air Cherenkov telescopes are shown for comparison.

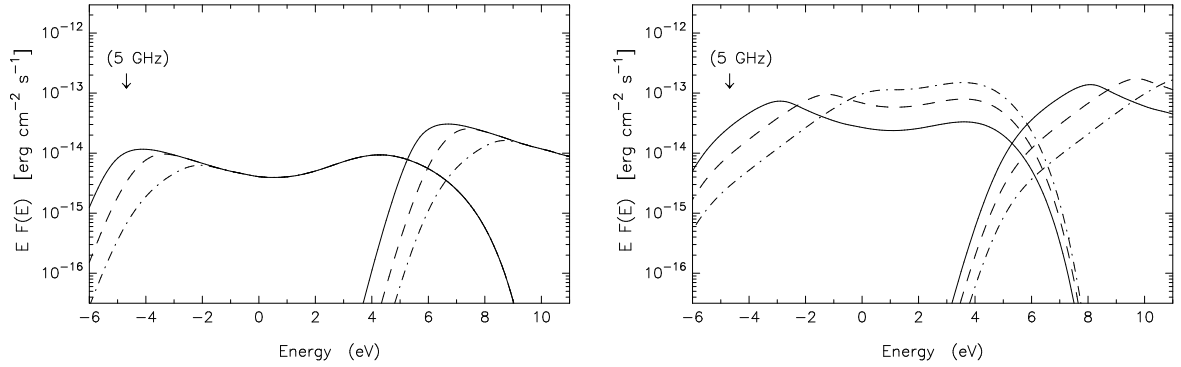


Fig. 2.— Numerical model for fluxes expected from blazar jets at comoving times $t' = 10^4$ yr (dot-dashed curves), 5×10^4 yr (dashed curves), and $t' = 3 \times 10^5$ yr (solid curves) after the start of injection event. (a) Numerical model for fluxes expected from a distant ($z = 1$) blazar jet with stationary injection of electrons in a relativistic knot for $B = 30 \mu\text{G}$, $\Gamma = 10$, $\theta = 2/\Gamma = 11.4^\circ$, $L = 10^{44} \text{ erg s}^{-1}$, and $\gamma_{max} = 8.5 \times 10^9$, corresponding to $e_{max} = 1$. (b) Fluxes from a close blazar ($z = 0.15$) for $\Gamma = 5$, $B = 6 \mu\text{G}$, $\theta = 23^\circ$, and $\gamma_{max} = 2 \times 10^9$, corresponding to $e_{max} = 0.01$. A gradually decreasing power of injection, with $q = 0.5$, $t_{inj} = 5 \times 10^3$ yr, and an initial luminosity $L_{44} = 5$ is supposed.